Volume 19 | Number 3 | 21 January 2017 | Pages 395–594

CrystEngComm

rsc.li/crystengcomm

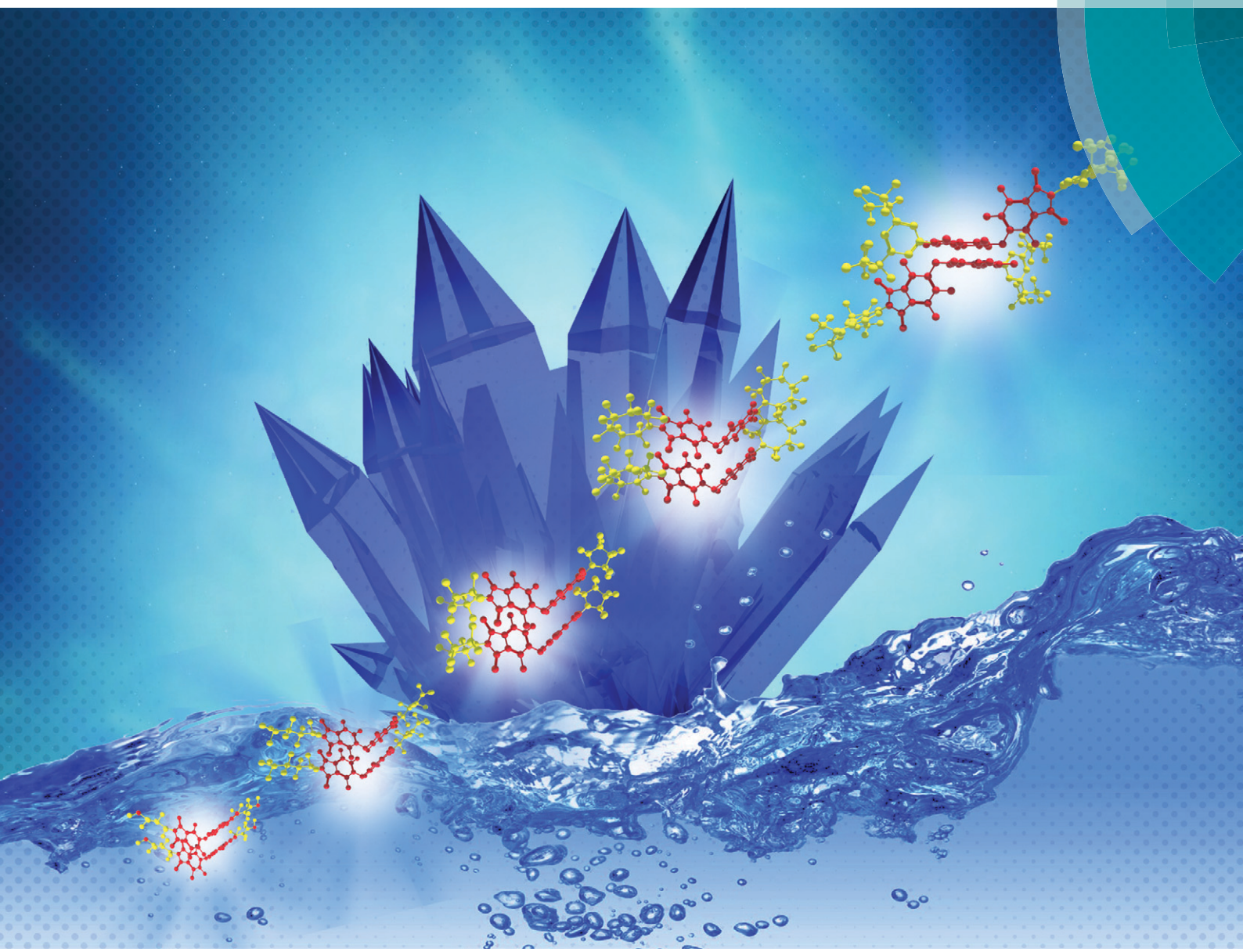

ROYAL SOCIETY OF CHEMISTRY

PAPER

Mahesh Hariharan *et al.*

V-shaped oxydiphthalimides: side-chain engineering regulates crystallisation-induced emission enhancement

CrystEngComm

PAPER

View Article Online
View Journal | View Issue

Cite this: *CrystEngComm*, 2017, **19**, 419

V-shaped oxydiphthalimides: side-chain engineering regulates crystallisation-induced emission enhancement†

Gopika Gopan,‡ P. S. Salini,‡ Somadrita Deb and Mahesh Hariharan*

Received 9th August 2016,
Accepted 24th October 2016

DOI: 10.1039/c6ce01738j

www.rsc.org/crystengcomm

Tuning the luminescence properties of solid state materials by controlling the molecular packing in the crystal has played an important role in designing new functional materials. A series of five V-shaped oxydiphthalimides (ODPs) were synthesised. Side-chain engineering has been successfully utilized to systematically tune their luminescence properties in the crystalline state by introducing sterically bulky side-chains at the imidic nitrogen. Fluorescence spectroscopy and single crystal X-ray analyses disclose the effect of conformational twisting and bulkiness of imidic substituents on crystallisation-induced emission enhancement (CIEE). Detailed analysis revealed that the CIEE factor of ODPs shows a linear dependence on the percentage volume of the side-chain.

Introduction

Organic luminescent materials have gained much attention in recent years owing to their potential applications in the fields of light emitting diodes (OLEDs),[1] solid state lasers,[2] sensors,[3] labels[4] and thin film transistors (OTFT).[5] The development of efficient solid state emitters from organic fluorophores is a challenging yet desirable task in optoelectronics. In most cases, organic dyes with high fluorescence quantum yields in the solution state do not show any detectable emission in the solid state due to the formation of excimers and exciplexes.[6] The last few decades have witnessed the emergence of a new class of functional materials with aggregation-induced emission enhancement (AIE/AIEE) characteristics, wherein the aggregated state of molecules was found to show emission efficiency much higher than that in the solution state.[7] The number of molecules that show enhanced emission in the crystalline state remains to be exiguous.[8] Due to strong π–π stacking interactions in the crystalline state, non-radiative decay is more probable to occur.[8,9] Since crystalline films show alluring charge mobility while constructing light-emitting diodes, researchers are in perpetual quest for luminescent materials that show crystallisation-induced emission enhancement (CIEE).[10] Since a close packed arrangement of molecules in the crystalline state inevitably, in most cases, quenches emission, it is highly essential to develop a strategy to enhance the luminescence of a crystalline material by manipulating the interactions at the molecular level.[11] The mechanism of CIEE is ascribed to the twisted conformation of the molecules in the crystalline state that prevents strong intermolecular π–π interaction. Restricted intramolecular rotations in the crystalline state can also contribute to CIEE. As a consequence, the photoexcited luminogens decay to the ground state through radiative pathways thus boosting the fluorescence emission.[12] Such an understanding about the structure–property correlation can serve as a basis for designing newer and better efficient solid state luminescent materials for practical applications. Constant efforts in this direction have given rise to many useful covalent[13] and non-covalent[14] synthesis strategies that can be used to develop organic crystalline materials with significant emission efficiency. Introduction of alkyl/aryl side-chains around the luminescent core can effectively perturb the electronic coupling between the chromophores. Albeit many reports on the effect of flexible side-chains on the device performance of OFETs and solar cells,[15] the possibilities of tuning solid state luminescence properties using side-chain engineering have received less attention.[16]

Our continued efforts to understand the photophysical properties of crystalline/assembled ryleneimides such as naphthalimide[17] and perylenimide[18] prompted us to explore the properties of their lower analogue, phthalimide. Herein, we introduce oxydiphthalimides (ODPs) as potential candidates for the aforementioned CIEE family. Although ODPs have been extensively studied for building polyimides and copolyimides,[19] their photophysical properties are hitherto

School of Chemistry, Indian Institute of Science Education and Research Thiruvananthapuram, CET Campus, Sreekaryam, Thiruvananthapuram, Kerala, India 695016. E-mail: mahesh@iisertvm.ac.in

† Electronic supplementary information (ESI) available: ^{1}H NMR and ^{13}C NMR of ODP1–5. CCDC 1490507–1490511. For ESI and crystallographic data in CIF or other electronic format see DOI: 10.1039/c6ce01738j

‡ These authors contributed equally.

unknown in the literature. With continuous endeavours to construct solid state luminescent materials,[20] in this work, we reveal the effect of the molecular structure, conformational twisting and solid state packing on the CIEE process of a series of ODPs *via* side-chain engineering of the imide moiety. We herein report the first example of exercising side-chain engineering on a V-shaped chromophore to obtain a linear dependence of CIEE on the bulkiness of the chosen side-chains.

Experimental section

Materials and methods

4,4′-Oxydiphthalic anhydride (95%), hydroxypropyl amine, *n*-propyl amine, cyclopentyl amine, cycloheptyl amine and 2,6-diisopropylaniline (97%) were purchased from Sigma Aldrich and used as such without further purification. Thin layer chromatography (TLC) analysis was performed on pre-coated aluminum plates of silica gel 60 F254 plates (0.25 mm, Merck), and the developed TLC plates were visualized under short and long wavelength UV lamps. Flash column chromatography was performed using silica gel of 200–400 mesh employing a solvent polarity correlated with the TLC mobility observed for the substance of interest. Yields refer to chromatographically and spectroscopically homogeneous substances. Melting points (m.p.) were obtained using a capillary melting point apparatus and are reported without correction. Photophysical measurements of the derivatives were carried out in a cuvette of 3 mm path length unless otherwise mentioned. Absorption and emission spectra were recorded on Shimadzu UV-3600 UV-VIS-NIR and Horiba Jobin Yvon Fluorolog spectrometers, respectively. Lifetime measurements were carried out on an IBH picosecond time correlated single photon counting (TCSPC) system. The pulse width of the excitation (λ_{exc} = 340 nm) source is determined to be <100 ps. The fluorescence decay profiles were deconvoluted using IBH data station software version 2.1, and fitted with exponential decay, minimizing the χ^2 values. 10 μM solutions of ODP1–5 in $CHCl_3$ were used for solution based photophysical measurements unless otherwise mentioned.

General procedure for the syntheses of ODP1–5 from 4,4′-oxydiphthalic anhydride (ODPA)

3.15 g (0.01 mol) of 4,4′-oxydiphthalic anhydride (ODPA) and 40 mL of acetic acid were added to a 100 mL two-neck round bottom flask equipped with a condenser and a mechanical stirrer. After ODPA dissolves in acetic acid, 0.022 mol of amine was added dropwise. The mixture was refluxed for 5–8 h at 120 °C, then cooled to room temperature and poured into cold water (Fig. 1a). The precipitate was collected using vacuum filtration and then purified using column chromatography. The respective oxydiphthalimides (ODPs) were obtained as white solids in 60–80% yields. Slow evaporation of ODPs from varying compositions of the chloroform : hexane mixture yielded colourless solvent-free crystals (Fig. 1b). ODP1–5 were characterized by spectroscopic and analytical

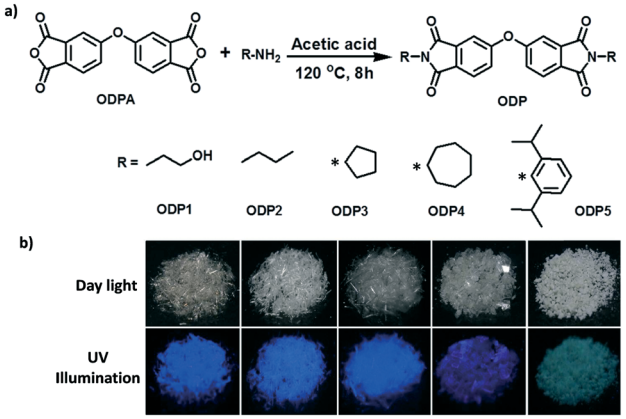

Fig. 1 a) Syntheses of oxydiphthalimides (ODP1, ODP2, ODP3, ODP4 and ODP5) from oxydiphthalic anhydride; b) photographic images of the crystals of ODP1, ODP2, ODP3, ODP4 and ODP5 in daylight and under UV illumination.

techniques and their structures were confirmed by single crystal X-ray diffraction analysis. ODP1–5 crystallized in a monoclinic crystal system with ODP1–4 belonging to the same space group ($C2/c$) while ODP5 belongs to $P2_1/c$ (Table 1).

ODP1 (yield = 75%): m.p. 156–157 °C; ^{1}H NMR (500 MHz, $CDCl_3$): δ = 7.83 (d, J = 8.1 Hz, 2H), 7.36 (s, 2H), 7.32 (d, J = 8.1, 2H), 3.79 (t, J = 6.4 Hz, 4H), 3.57 (q, J = 5.9, 4H), 2.28 (t, J = 6.33, 2H), 1.85–1.79 (m, 4H); ^{13}C NMR (125 MHz, $CDCl_3$): δ = 164.82, 159.25, 131.83, 127.52, 125.98, 119.73, 115.75, 60.25, 38.16, 32.05; IR (KBr): 3510, 3071, 2938, 2884, 1761, 1695, 1612, 1477, 1441, 1395, 1265, 1229, 1123, 1072, 934, 858, 748 cm^{-1}; HR-MS (EI)-(m/z): 424.1327; anal. calcd. for $C_{22}H_{20}N_2O_7$: C, 62.26; H, 4.75; N, 6.60; found: C, 62.19; H, 4.54; N, 6.40.

ODP2 (yield = 68%): m.p. 148–149 °C; ^{1}H NMR (500 MHz, $CDCl_3$): δ = 7.8 (d, J = 8.0 Hz, 2H), 7.35 (s, 2H), 7.29 (d, J = 8.0, 2H), 3.61 (t, J = 7.5 Hz, 4H), 1.56–1.61 (m, 4H), 1.28–1.32 (m, 4H), 0.88 (t, J = 7.5 Hz, 6H); ^{13}C NMR (125 MHz, $CDCl_3$): δ = 164.91, 160.17, 132.26, 127.35, 124.92, 119.64, 115.14, 40.97, 31.59, 20.18, 13.97; IR (KBr): 3071, 2965, 2929, 2870, 1778, 1722, 1607, 1470, 1369, 1273, 1231, 1105, 835, 748 cm^{-1}; HR-MS (EI)-(m/z): 420.1738; anal. calcd. for $C_{24}H_{24}N_2O_5$: C, 68.56; H, 5.75; N, 6.66; found: C, 69.05; H, 5.63; N, 6.52.

ODP3 (yield = 70%): m.p. 163–164 °C. ^{1}H NMR (500 MHz, $CDCl_3$): δ = 7.86 (d, J = 8.0 Hz, 2H), 7.41 (s, 2H), 7.35 (d, J = 8.0, 2H), 4.60–4.67 (m, 2H), 2.11–2.13 (m, 8H), 1.63–1.67 (m, 8H); ^{13}C NMR (125 MHz, $CDCl_3$): δ = 165.34, 158.56, 131.48, 127.73, 125.19, 119.92, 116.47, 42.82, 28.06, 19.38; IR (KBr): 3071, 2936, 2866, 1767, 1705, 1612, 1477, 1439, 1393, 1356, 1261, 1227, 1173, 1088, 1051, 945, 853, 748 cm^{-1}; HR-MS (EI)-(m/z): 444.1756; anal. calcd. for $C_{26}H_{24}N_2O_5$: C, 70.26; H, 5.44; N, 6.30; found: C, 70.81; H, 5.39; N, 6.04.

ODP4 (yield = 77%): m.p. 153–154 °C. ^{1}H NMR (500 MHz, $CDCl_3$): δ = 7.83 (d, J = 8.1 Hz, 2H), 7.38 (s, 2H), 7.33 (d, J = 8.1, 2H), 4.23–4.27 (m, 2H), 1.79–1.82 (m, 8H), 1.51–1.65 (m, 16H); ^{13}C NMR (125 MHz, $CDCl_3$): δ = 164.85, 158.39, 131.02, 126.70, 123.51, 121.84, 117.29, 42.16, 33.47, 30.05, 25.13; IR

Table 1 Crystallographic data and refinement parameters for crystalline ODP1–5

	ODP1	ODP2	ODP3	ODP4	ODP5
Empirical formula	$C_{22}H_{20}N_2O_7$	$C_{24}H_{24}N_2O_5$	$C_{26}H_{24}N_2O_5$	$C_{30}H_{32}N_2O_5$	$C_{40}H_{40}N_2O_5$
Formula weight (g)	424.40	420.46	444.48	500.59	628.76
Color, shape	Colorless, block	Colorless, block	Colorless, rectangular	Colorless, rectangular	Colorless, block
Temperature (K)	296	296	296	296	296
Crystal system	Monoclinic	Monoclinic	Monoclinic	Monoclinic	Monoclinic
Space group	*C*2/*c*	*C*2/*c*	*C*2/*c*	*C*2/*c*	$P2_1/c$
a (Å)	16.685	16.477	43.489	32.385	13.856
b (Å)	5.027	5.156	5.242	5.311	20.531
c (Å)	22.863	24.853	19.472	5.679	13.634
α (deg)	90	90	90	90	90
β (deg)	96	92.79	104.45	110.53	116.97
γ (deg)	90	90	90	90	90
Volume (Å^3)	1907.07	2109.00	4298.70	2526.00	3456.80
Z	4	4	8	4	4
Density (calculated)	1.479	1.323	1.373	1.310	1.207
No. of reflections collected	7046	8056	18 882	9708	26 924
No. of unique reflections	1666	2160	1927	9708	6085
No. of parameters	142	141	298	170	424
R_1, wR_2 [$I > 2$sigma(I)]	0.0344, 0.0843	0.0612, 0.1761	0.0440, 0.1275	0.0726, 0.2056	0.0554, 0.1462
R_1, wR_2 (all data)	0.0421, 0.0910	0.0782, 0.1902	0.0620, 0.1608	0.0952, 0.2360	0.1039, 0.1906
Absorption coefficient	0.112	0.093	0.096	0.090	0.079
F(000)	888	888	1872	1056	1336
Goodness of fit	1.036	1.057	1.141	1.046	1.063
CCDC number	1490507	1490508	1490509	1490510	1490511

(KBr): 2953, 2872, 1767, 1703, 1612, 1474, 1373, 1265, 1231, 1088, 748 cm^{-1}; HR-MS (EI)-(*m*/*z*): 500.2381; anal. calcd. for $C_{30}H_{32}N_2O_5$: C, 71.98; H, 6.44; N, 5.60; found: C, 72.46; H, 6.30; N, 5.34.

ODP5 (yield = 63%): m.p. 210–211 °C. 1H NMR (500 MHz, $CDCl_3$): δ = 7.97 (d, J = 8.0 Hz, 2H), 7.50 (s, 2H), 7.48 (d, J = 8.5 Hz, 4H), 7.41 (t, J = 8.0 Hz, 2H), 7.23 (d, J = 8.0 Hz, 2H), 2.63–2.69 (m, 4H), 1.14 (d, J = 11, 24H); ^{13}C NMR (125 MHz, $CDCl_3$): δ = 162.86, 159.18, 142.94, 134.82, 130.24, 126.09, 123.93, 122.40, 122.02, 121.17, 115.89, 25.14, 23.26; IR (KBr): 2924, 2859, 1767, 1701, 1609, 1470, 1435, 1368, 1261, 1227, 1090, 847, 746 cm^{-1}; HR-MS (EI)-(*m*/*z*): 628.2914; anal. calcd. for $C_{40}H_{40}N_2O_5$: C, 76.41; H, 6.41; N, 4.46; found: C, 76.56; H, 6.45; N, 4.06.

Results and discussion

A series of five oxydiphthalimides (ODP1–5), which differ in the substituents at imidic nitrogen, were synthesised using condensation reaction of oxydiphthalic anhydride with various amines as per the procedure outlined in Fig. 1a. The amines were chosen in such a way that there is a systematic increase in the bulkiness of the alkyl/aryl group attached to nitrogen. Single crystal X-ray diffraction analysis revealed that ODP1–5 displayed twisted structures, with a V-shape geometry, in which the phthalimide rings are nearly orthogonal to each other with angle between their planes being 77.40° (ODP1), 74.48° (ODP2), 76.69° (ODP3), 70.08° (ODP4) and 74.95° (ODP5) (Fig. 2). Furthermore, in the case of ODPs with bulky side-chains (ODP3–5), the dihedral angle between the phthalimide ring and the bulky substituents is 87.52° (ODP3), 85.77° (ODP4) and 87.15° (ODP5), respectively, suggesting a near orthogonal arrangement (Fig. S1, ESI†). In ODP1–4, steric inhibition arising from such a geometrical arrangement tends to maintain a certain distance between the phthalimide units of adjacent molecules (Fig. 3a). Such an arrangement suppresses the close packing and π–π intermolecular interactions, thereby inhibiting the face to face interaction in ODP1–4. Top and side views (Fig. 4 and 5) of the neighbouring molecular pair in crystalline ODP1–4 show that the phthalimide rings of neighbouring molecules do not stack on top of each other. Introduction of the bulky 2,6-diisopropylphenyl moiety on the imidic nitrogen brought about considerable changes in crystalline ODP5. The ODP5 molecule adopts an entirely different packing arrangement in the crystal with each pair of

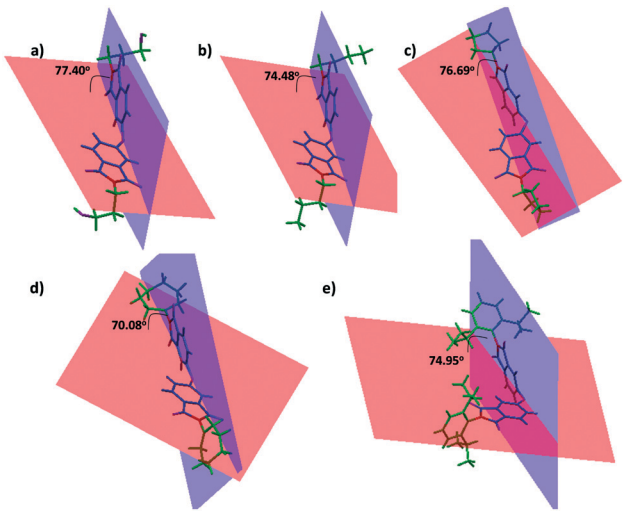

Fig. 2 Angles between the planes of phthalimide units in the crystal packing of a) ODP1, b) ODP2, c) ODP3, d) ODP4 and e) ODP5.

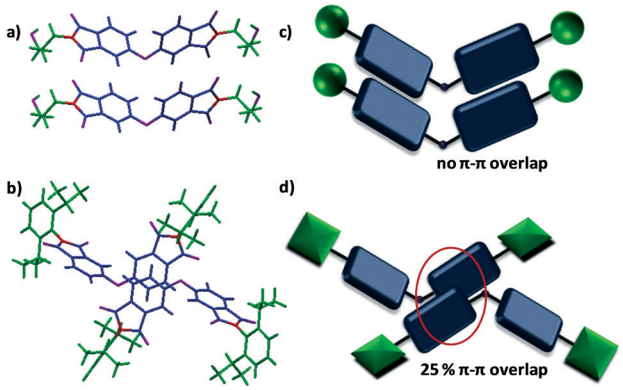

Fig. 3 Arrangement of the nearest neighbours of a) ODP1 and b) ODP5 in the crystal; schematic models of the nearest neighbours of c) ODP1 and d) ODP5 showing the difference in packing and the consequent π–π interaction induced by the bulky side-chain in ODP5.

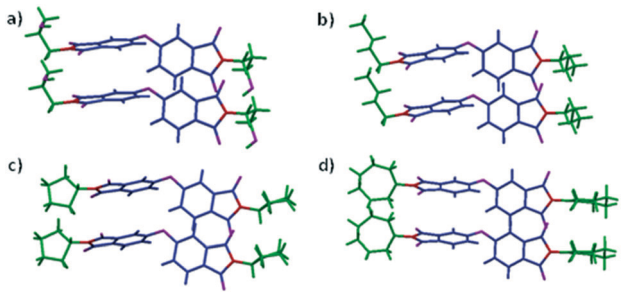

Fig. 4 Top view of a) ODP1, b) ODP2, c) ODP3 and d) ODP4 exhibiting a negligible aerial overlap between the phthalimide units in close packing.

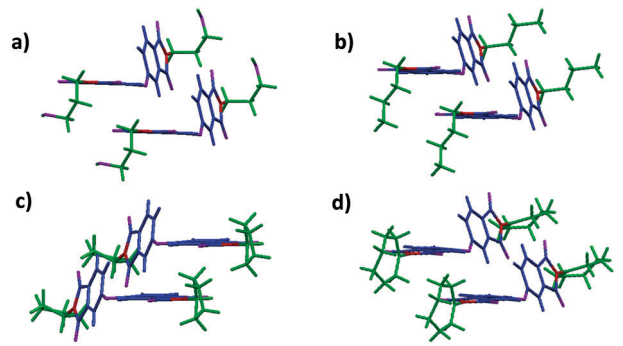

Fig. 5 Side view of a) ODP1, b) ODP2, c) ODP3 and d) ODP4 exhibiting a negligible aerial overlap between the phthalimide units in close packing.

neighbouring molecules forming a dimer (Fig. 3b), facilitated by the π–π interaction between phthalimide units. The arrangement of the nearest neighbours in ODP1, as a representative example of ODP1–4, and ODP5 is depicted in Fig. 3c and d. The figure clearly shows the π–π interaction aided by the bulky side-chain in ODP5 which results in a 25% π–π overlap. In crystalline ODP1–5, C···O, O···H and O···O interactions act as the principal driving forces for the molecular packing (Fig. S2–S6, ESI†). The combined effects of such weak interactions fix the molecular conformation of ODP1–5 in the crystalline state.

The steady state absorption spectra of ODP1–5 in chloroform exhibited a band centered at 233 nm (Table 2; Fig. S7, ESI†), with a tail extending up to 350 nm. Analysis of the absorption spectrum shows that the peak positions are independent of the imidic substituents. The absorption spectra are governed by the n to π* and π to π* transitions of the phthalimide core.[21] Upon excitation at 340 nm, ODP1–4 in chloroform exhibited a broad emission centered at 407 nm (Table 2; Fig. 6a; Fig. S8 and S9, ESI†) with quantum yields (Φ_f) of 23.6%, 5.7%, 4.4% and 3.4%, respectively (Table 2). ODP5 showed a notable difference in the emission spectra where a significant red-shifted band at 481 nm (Table 2; Fig. 6a; Fig. S9, ESI†) was observed with a quantum yield of 0.5%. Picosecond time-resolved fluorescence measurements of ODP1–5 in chloroform exhibit a monoexponential decay with short fluorescence lifetimes (τ = 1.89–10.53 ns) (Fig. 6b; Table 2) when monitored at respective emission maxima upon excitation at 340 nm. The red shift in the emission spectra as well as the observed lower fluorescence quantum yield of ODP5 is indicative of twisted intramolecular charge transfer (TICT)[10b] in solution. Solvent dependent studies of ODP5 (Fig. S10a, ESI†) show a red shift in the emission maximum (457 nm to 491 nm) with the increase in polarity of the solvent from cyclohexane to acetonitrile. With further increase in the solvent polarity, the emission got quenched. Similar studies were carried out in the case of ODP2 for comparison, but a solvent dependent shift in the emission maximum was not observed (Fig. S10b, ESI†). The difference between the excited- and ground-state dipole moments in ODP5 is estimated to be 5.65 D employing the Lippert–Mataga equation (Fig. S10c, ESI†). Frontier molecular orbital (FMO) analysis (Fig. 6c; Table S1, ESI†) shows that the electron density of the HOMO and LUMO is distributed throughout the whole molecule in ODP1–4. However, in the case of ODP5, the electron density is completely concentrated on the 2,6-diisopropylphenyl moiety in the HOMO, whereas in the LUMO, complete localization of the electron density is on the phthalimide moiety. The FMOs calculated for the representative dimer pair in ODP5 exhibit a similar feature to that of monomeric ODP5 (Table S1, ESI†). The FMO analysis, in addition to the solvent polarity dependence of emission maxima, is clearly indicative of the TICT between the phthalimide unit and the imide moiety in the ground state of ODP5.

In the crystalline state, the diffuse reflectance absorption spectra of ODP1–5 showed a band around 340–360 nm which is red shifted compared to that in the solution state (Table 2; Fig. S7, ESI†). Upon excitation at 340 nm, ODP1–2 showed a band at 387 nm, whereas ODP3–5 showed bands at 391 nm, 403 nm and 411 nm, respectively (Fig. 6d; Table 2). As the bulkiness of the substituents at imidic nitrogen increases, a progressive red shift in the emission maximum of the crystalline ODP was observed. The fluorescence lifetime decay profiles of crystalline ODP1–5 follow a bi-exponential fit with a longer lifetime in addition to the lifetime corresponding to the monomer species (Fig. 6e; Table 2) when excited at 340

Table 2 Photophysical properties of ODP1–5 in the solution state ($CHCl_3$) and in the crystalline state

	$\lambda_{abs}{}^a$ (nm)	$\lambda_f{}^a$ (nm)	$\Phi_f{}^a$	$\tau_f{}^a$ (ns)	$k_r{}^a$ ($\times 10^6$)	$k_{nr}{}^a$ ($\times 10^6$)	$\lambda_{abs}{}^b$ (nm)	$\lambda_f{}^b$ (nm)	$\Phi_f{}^b$	$\tau_f{}^b$ (ns) [amplitude] (%)	$k_r{}^b$ ($\times 10^3$)	$k_{nr}{}^b$ ($\times 10^3$)	$\Phi_f{}^b/\Phi_f{}^a$
ODP1	234	407	0.236	10.17	0.048	0.157	361	388	0.267	10.06 [84], 179.86 [16]	1.880	5.190	1.132
ODP2	234	406	0.057	10.53	0.014	0.231	348	386	0.084	171.98 [29], 3.36 [71]	0.520	5.690	1.466
ODP3	234	409	0.044	8.23	0.009	0.203	347	391	0.097	6.65 [81], 108.21 [19]	1.113	10.370	2.220
ODP4	233	412	0.034	5.84	0.008	0.230	343	403	0.085	2.86 [62], 16.196 [38]	6.430	69.270	2.511
ODP5	232	482	0.005	1.89	0.002	0.350	341	411	0.020	5.65 [22], 173.72 [78]	0.116	5.690	4.320

[a] Chloroform solution. [b] Crystalline state; abs – absorption; f – fluorescence; the observed decrease in the rate of the radiative decay for crystalline ODP5 when compared to that for ODP5 in solution is indicative of the formation of the 'H' type aggregate.

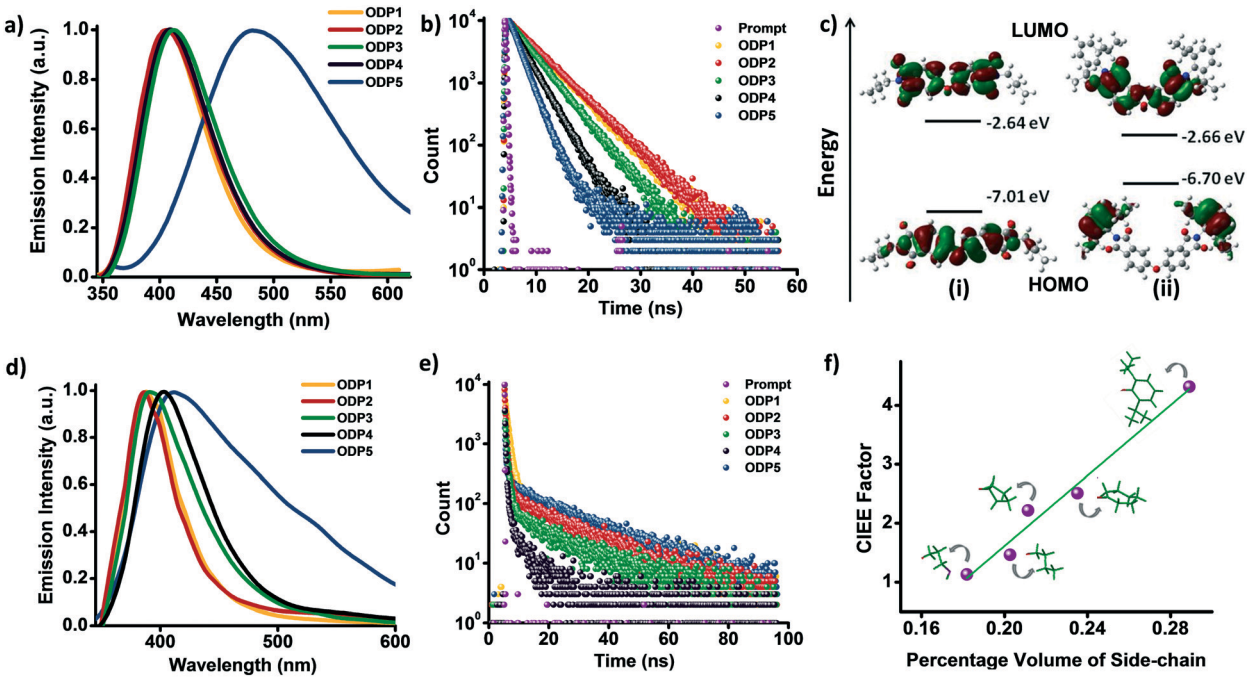

Fig. 6 Solution state a) fluorescence emission spectra and b) fluorescence decay profiles (λ_{exc} = 340 nm) of ODP1–5; c) molecular orbital amplitude plots of HOMO and LUMO energy levels of (i) ODP2 (as a representative example of ODP1–4) and (ii) ODP5 calculated by using the B3LYP/6-311+G (d,p) basis set; crystalline state d) fluorescence emission spectra and e) fluorescence decay profiles (λ_{exc} = 340 nm) of ODP1–5; f) plot of the CIEE factor ($\varphi_{f(crystal)}/\varphi_{f(solution)}$) *vs.* the percentage volume of the side-chain.

nm and monitored at the respective emission maxima. Lifetime analysis of crystalline ODP1–4 revealed that the major emissive component belongs to the monomeric species with the shorter lifetime. Steady state emission of crystalline ODP5 arises predominantly from the aggregated species having a longer lifetime. By virtue of the twisted conformation, ODP1–4 are devoid of H/J-aggregates. As a result, the crystalline state of ODP1–4 manifests a monomer-like emission. In contrast to ODP1–4, two phthalimide moieties in ODP5 from adjacent molecules form a dimer and adopt a face-to-face π-stacked arrangement with an interplanar separation ($d_{\pi-\pi}$) of 3.73 Å. The blue shift in the emission maxima in combination with the lower k_r value of crystalline ODP5 compared to that in the solution state indicates the possibility of H-like aggregates (Table 2). In ODP1–5, inhibition of the internal rotations due to the weak interactions in the crystal reduces non-radiative relaxation, thereby resulting in enhanced crystalline emission. The CIEE factor, which is the relative quantum yield values of the crystalline state with respect to the solution state ($\varphi_{f(crystal)}/\varphi_{f(solution)}$) of ODP1–5 (Table 2) was found to be 1.132, 1.466, 2.220, 2.511 and 4.320 for ODP1–5, respectively. The plot of the CIEE factor *vs.* percentage volume[22] of the side-chains (Fig. 6f) reflects a linear relationship between the enhancement in emission and the bulkiness of the side-chains on the imidic nitrogen. In contrast, we observed an increase in the aggregation-induced enhanced emission (AIEE) of ODPs with the decrease in the percentage volume of the side-chains (Fig. S11, ESI†).

Hirshfeld surface analysis provides additional insight into the molecular interactions of ODP1–5 (Table S2†). The strong C···H contacts including the C–H···π interactions comprise 18.1%, 17.0%, 16.6%, 13.6% and 17.5% of the total Hirshfeld surfaces for ODP1, ODP2, ODP3, ODP4 and ODP5, respectively, whereas the C···C interactions contribute 0.3%, 0.1%,

2.3%, 2.5% and 1.9%, respectively. In ODP1–5, the contribution of the contacts including the π–π interactions is negligible compared to the other interactions present in the crystal (Fig. S12, ESI†).

Conclusions

In summary, five V-shaped N-substituted oxydiphthalimides with varying imide side-chains are reported. Topological analyses revealed that the introduction of sterically bulky substituents around the luminescent core has increased the extent of close packing in the crystals. The relatively high quantum yield of crystalline ODP1–5 shows that ODPs are promising candidates for the CIEE family. Solvent dependent emission studies and FMO analysis are indicative of TICT in ODP5. Side-chain engineering was successfully utilised to obtain a linear relation between the volume of the side-chain and the order of emission enhancement from the solution state to the crystalline state. The strategy of regulating the luminescence properties of crystalline solids by varying the bulkiness of the side-chains at the molecular level could be exploited in the design and construction of organic luminescent materials. We believe that the facile synthesis and easy crystallising nature of ODP derivatives with CIEE characteristics will provide them a secured position as a new versatile class of luminogens.

Acknowledgements

M. H. acknowledges Kerala State Council for Science, Technology and Environment (KSCSTE) for the support of this work, 007/KSYSA-RG/2014/KSCSTE. The authors thank Alex P. Andrews, IISER-TVM for single crystal X-ray structure analyses. Gopika Gopan thanks INSPIRE Fellowship for the financial assistance.

Notes and references

1 (*a*) M. A. Baldo, D. F. O'Brien, Y. You, A. Shoustikov, S. Sibley, M. E. Thompson and S. R. Forrest, *Nature*, 1998, **395**, 151; (*b*) Y. Gong, J. Liu, Y. Zhang, G. He, Y. Lu, W. B. Fan, W. Z. Yuan, J. Z. Sun and Y. Zhang, *J. Mater. Chem. C*, 2014, **2**, 7552.

2 (*a*) X. Wang, Q. Liao, H. Li, S. Bai, Y. Wu, X. Lu, H. Hu, Q. Shi and H. Fu, *J. Am. Chem. Soc.*, 2015, **137**, 9289; (*b*) M. Wei, R. Huang, K. Guo, Y. Jing, T. Xu and B. Wei, *J. Mater. Chem. C*, 2014, **2**, 8131; (*c*) Z. Yu, Y. Wu, Q. Liao, H. Zhang, S. Bai, H. Li, Z. Xu, C. Sun, X. Wang, J. Yao and H. Fu, *J. Am. Chem. Soc.*, 2015, **137**, 15105.

3 (*a*) M. Wang, D. Zhang, G. Zhang and D. Zhu, *Chem. Commun.*, 2008, 4469; (*b*) J. Wu, W. Liu, J. Ge, H. Zhang and P. Wang, *Chem. Soc. Rev.*, 2011, **40**, 3483; (*c*) P. Mazumdar, D. Das, G. P. Sahoo, G. Salgado-Moran and A. Misra, *Phys. Chem. Chem. Phys.*, 2015, **17**, 3343; (*d*) P. Mazumdar, D. Das, G. P. Sahoo, G. Salgado-Moran and A. Misra, *Phys. Chem. Chem. Phys.*, 2014, **16**, 6283.

4 M. Bruchez, M. Moronne, P. Gin, S. Weiss and A. P. Alivisatos, *Science*, 1998, **281**, 2013.

5 (*a*) M. M. Durban, P. D. Kazarinoff, Y. Segawa and C. K. Luscombe, *Macromolecules*, 2011, **44**, 4721; (*b*) X. Guo, R. P. Ortiz, Y. Zheng, M.-G. Kim, S. Zhang, Y. Hu, G. Lu, A. Facchetti and T. J. Marks, *J. Am. Chem. Soc.*, 2011, **133**, 13685; (*c*) Y. Zhou, W.-J. Liu, Y. Ma, H. Wang, L. Qi, Y. Cao, J. Wang and J. Pei, *J. Am. Chem. Soc.*, 2007, **129**, 12386.

6 Z. Xie, B. Yang, F. Li, G. Cheng, L. Liu, G. Yang, H. Xu, L. Ye, M. Hanif, S. Liu, D. Ma and Y. Ma, *J. Am. Chem. Soc.*, 2005, **127**, 14152.

7 (*a*) J. Luo, Z. Xie, J. W. Y. Lam, L. Cheng, H. Chen, C. Qiu, H. S. Kwok, X. Zhan, Y. Liu, D. Zhu and B. Z. Tang, *Chem. Commun.*, 2001, 1740; (*b*) B.-K. An, S.-K. Kwon, S.-D. Jung and S. Y. Park, *J. Am. Chem. Soc.*, 2002, **124**, 14410.

8 J. Tong, Y. J. Wang, Z. Wang, J. Z. Sun and B. Z. Tang, *J. Phys. Chem. C*, 2015, **119**, 21875.

9 (*a*) Z. Chen, J. Zhang, M. Song, J. Yin, G.-A. Yu and S. H. Liu, *Chem. Commun.*, 2015, **51**, 326; (*b*) Y. Lin, G. Chen, L. Zhao, W. Z. Yuan, Y. Zhang and B. Z. Tang, *J. Mater. Chem. C*, 2015, **3**, 112; (*c*) C. Yang, Q. T. Trinh, X. Wang, Y. Tang, K. Wang, S. Huang, X. Chen, S. H. Mushrif and M. Wang, *Chem. Commun.*, 2015, **51**, 3375.

10 (*a*) Y. Dong, J. W. Y. Lam, A. Qin, Z. Li, J. Sun, H. H. Y. Sung, I. D. Williams and B. Z. Tang, *Chem. Commun.*, 2007, 40; (*b*) T. Han, X. Feng, D. Chen and Y. Dong, *J. Mater. Chem. C*, 2015, **3**, 7446.

11 Y.-X. Li, X.-F. Yang, J.-L. Miao, Z.-W. Zhang and G.-X. Sun, *CrystEngComm*, 2016, **18**, 2098.

12 B. Z. Tang and A. Qin, *Aggregation-Induced Emission: Fundamentals*, Wiley, 2013.

13 S. Mukherjee and P. Thilagar, *Proc. Natl. Acad. Sci., India, Sect. A*, 2014, **84**, 131.

14 (*a*) D. Yan, H. Yang, Q. Meng, H. Lin and M. Wei, *Adv. Funct. Mater.*, 2014, **24**, 587; (*b*) G. Fan, X. Yang, R. Liang, J. Zhao, S. Li and D. Yan, *CrystEngComm*, 2016, **18**, 240; (*c*) S. Li, Y. Lin and D. Yan, *J. Mater. Chem. C*, 2016, **4**, 2527.

15 (*a*) F. Zhang, Y. Hu, T. Schuettfort, C.-a. Di, X. Gao, C. R. McNeill, L. Thomsen, S. C. B. Mannsfeld, W. Yuan, H. Sirringhaus and D. Zhu, *J. Am. Chem. Soc.*, 2013, **135**, 2338; (*b*) X.-Y. Wang, F.-D. Zhuang, X. Zhou, D.-C. Yang, J.-Y. Wang and J. Pei, *J. Mater. Chem. C*, 2014, **2**, 8152; (*c*) J. Y. Back, T. K. An, Y. R. Cheon, H. Cha, J. Jang, Y. Kim, Y. Baek, D. S. Chung, S.-K. Kwon, C. E. Park and Y.-H. Kim, *ACS Appl. Mater. Interfaces*, 2015, **7**, 351.

16 (*a*) S. Sekiguchi, K. Kondo, Y. Sei, M. Akita and M. Yoshizawa, *Angew. Chem., Int. Ed.*, 2016, **55**, 6906; (*b*) J. Mei and Z. Bao, *Chem. Mater.*, 2014, **26**, 604.

17 A. R. Mallia, P. S. Salini and M. Hariharan, *J. Am. Chem. Soc.*, 2015, **137**, 15604.

18 (*a*) R. T. Cheriya, A. R. Mallia and M. Hariharan, *Energy Environ. Sci.*, 2014, **7**, 1661; (*b*) R. T. Cheriya, K. Nagarajan and M. Hariharan, *J. Phys. Chem. C*, 2013, **117**, 3240.

19 P. Thiruvasagam and B. Saritha, *J. Polym. Res.*, 2015, **22**, 1.

20 (*a*) S. K. Rajagopal, A. M. Philip, K. Nagarajan and M. Hariharan, *Chem. Commun.*, 2014, **50**, 8644; (*b*) S. K. Rajagopal, V. S. Reddy and M. Hariharan, *CrystEngComm*, 2016, **18**, 5089; (*c*) A. R. Mallia, R. Sethy, V. Bhat and M. Hariharan, *J. Mater. Chem. C*, 2016, **4**, 2931.

21 V. Wintgens, P. Valat, J. Kossanyi, L. Biczok, A. Demeter and T. Berces, *J. Chem. Soc., Faraday Trans.*, 1994, **90**, 411.

22 The bulkiness of the side-chains attached to the phthalimide core in ODP1–5 is associated directly with the relative volume of the side-chains with respect to the whole molecule (percentage volume) in each case. The volume of the required fragments was determined quantitatively using Crystal Explorer 2.1.